J|A|C|S
ARTICLES
Published on Web 07/25/2006

Experimental and Theoretical Studies of ^{45}Sc NMR Interactions in Solids

Aaron J. Rossini and Robert W. Schurko*

Contribution from the Department of Chemistry and Biochemistry, University of Windsor, Windsor, Ontario, Canada N9B 3P4

Received January 20, 2006; E-mail: rschurko@uwindsor.ca

Abstract: Solid-state ^{45}Sc NMR spectroscopy, ab initio calculations, and X-ray crystallography are applied to examine the relationships between ^{45}Sc NMR interactions and molecular structure and symmetry. Solid-state ^{45}Sc ($I = 7/2$) magic-angle spinning (MAS) and static NMR spectra of powdered samples of Sc(acac)$_3$, Sc(TMHD)$_3$, Sc(NO$_3$)$_3$·5H$_2$O, Sc(OAc)$_3$, ScCl$_3$·6H$_2$O, ScCl$_3$·3THF, and ScCp$_3$ have been acquired. These systems provide a variety of scandium coordination environments yielding an array of distinct ^{45}Sc chemical shielding (CS) and electric field gradient (EFG) tensor parameters. Acquisition of spectra at two distinct magnetic fields allows for the first observations of scandium chemical shielding anisotropy (CSA). ^{45}Sc quadrupolar coupling constants (C_Q) range from 3.9 to 13.1 MHz and correlate directly with the symmetry of the scandium coordination environment. Single-crystal X-ray structures were determined for Sc(TMHD)$_3$, ScCl$_3$·6H$_2$O, and Sc(NO$_3$)$_3$·5H$_2$O to establish the hitherto unknown scandium coordination environments. A comprehensive series of ab initio calculations of EFG and CS tensor parameters are in excellent agreement with the observed parameters. Theoretically determined orientations of the NMR interaction tensors allow for correlations between NMR tensor characteristics and scandium environments. Solid-state ^{45}Sc, ^{13}C, and ^{19}F NMR experiments are also applied to characterize the structures of the microcrystalline Lewis acid catalyst Sc(OTf)$_3$ (for which the crystal structure is unknown) and a noncrystalline, microencapsulated, polystyrene-supported form of the compound.

Introduction

The chemistry of scandium has not been explored to the extent of other transition metals due to the relatively high costs of materials and its limited reactivity arising from restriction to the +3 oxidation state. The use of scandium in both inorganic and organometallic chemistry has recently received more attention, as observed by the increasing number of compounds that have been synthesized and characterized by single-crystal X-ray diffraction and other methods.[1,2] Scandium is found in an assortment of materials, such as alloys,[3] inorganic materials,[4−9] ferroelectric relaxors, and ceramics.[10−15] Scandium complexes are also used in a number of organic syntheses and polymerization reactions. Certain Sc(III) complexes, due to the extreme electron deficiency at the Sc atom, act as some of the strongest Lewis acids among transition metal complexes. For instance, scandium triflate is extensively used in organic synthesis to catalyze a wide variety of reactions.[16,17] There is also increasing interest in the organometallic chemistry of scandium, since Sc−C bonds are especially susceptible to insertion reactions involving unsaturated molecules. Active scandium catalysts for the copolymerization of ethylene with styrene or norbornene have been synthesized.[18,19] Further advances have also been made with the incorporation of non-cyclopentadienyl ligand systems.[20,21] Given the increased interest in scandium chemistry, development of solid-state ^{45}Sc NMR spectroscopy for characterization of molecular structure and dynamics in both crystalline and disordered materials is of great importance.

Scandium has one naturally occurring NMR active isotope, ^{45}Sc, which is 100% naturally abundant, possesses a gyromagnetic ratio of 6.50880×10^7 rad T^{-1} s^{-1} (close to ^{13}C), a nuclear spin of $I = 7/2$, and a moderate nuclear quadrupole moment (Q) of 0.22×10^{-28} m^2. These factors result in a relative receptivity of 1780 in comparison to ^{13}C, making ^{45}Sc an excellent nucleus for NMR experimentation. Solid-state ^{45}Sc

(1) Cotton, S. A. *Polyhedron* **1999**, *18*, 1691.
(2) Meehan, P. R.; Aris, D. R.; Willey, G. R. *Coord. Chem. Rev.* **1999**, *181*, 121.
(3) Royset, J.; Ryum, N. *Int. Mater. Rev.* **2005**, *50*, 19.
(4) Park, H. S.; Bull, I.; Peng, L. M.; Victor, G. Y. J.; Grey, C. P.; Parise, J. B. *Chem. Mater.* **2004**, *16*, 5350.
(5) Napper, J. D.; Layland, R. C.; Smith, M. D.; zur Loye, H. C. *J. Chem. Crystallogr.* **2004**, *34*, 347.
(6) Perles, J.; Iglesias, M.; Ruiz-Valero, C.; Snejko, N. *J. Mater. Chem.* **2004**, *14*, 2683.
(7) Kolitsch, U.; Tillmanns, E. *Eur. J. Mineral.* **2004**, *16*, 143.
(8) Kolitsch, U.; Tillmanns, E. *Mineral. Magn.* **2004**, *68*, 677.
(9) Brigden, C. T.; Thompsett, D.; Williams, C. D. *Dalton Trans.* **2004**, 2829.
(10) Yue, X.; Xiao, D. Q.; Cao, J.; Yuan, X. W.; Yu, G. L.; Xiong, X. B.; Wei, L.; Zhu, J. G. *Ceram. Int.* **2004**, *30*, 1905.
(11) Yamashita, Y. J.; Hosono, Y. *Jpn. J. Appl. Phys., Part 1* **2004**, *43*, 6679.
(12) Pietraszko, A.; Hilczer, B.; Caranoni, C. *Ferroelectrics* **2004**, *298*, 235.
(13) Yoshikawa, Y.; Hanada, T.; Kogai, T. *J. Eur. Ceram. Soc.* **2004**, *24*, 1041.
(14) Maignan, A.; Pelloquin, D.; Flahaut, D.; Caignaert, V. *J. Solid State Chem.* **2004**, *177*, 3693.
(15) Kurama, S.; Mandal, H. *Key Eng. Mater.* **2004**, *264−268*, 1107−1110.
(16) Kobayashi, S. *Eur. J. Org. Chem.* **1999**, *1999*, 15.
(17) Kobayashi, S.; Nagayama, S. *J. Am. Chem. Soc.* **1998**, *120*, 2985.
(18) Li, X. F.; Baldamus, J.; Hou, Z. *Angew. Chem., Int. Ed.* **2005**, *44*, 962.
(19) Luo, Y. J.; Baldamus, J.; Hou, Z. M. *J. Am. Chem. Soc.* **2004**, *126*, 13910.
(20) Piers, W. E.; Emslie, D. J. H. *Coord. Chem. Rev.* **2002**, *233*, 131.
(21) Mountford, P.; Ward, B. D. *Chem. Commun.* **2003**, 1797.

NMR spectra are normally comprised of relatively broad powder patterns which result from anisotropic NMR interactions. The quadrupolar interaction (QI) normally determines the appearance of such spectra, though the effects of chemical shielding anisotropy (CSA) also significantly influence the appearance of the spectra. $^{1}H-^{45}Sc$ dipolar coupling can be observed in some instances. While the presence of these interactions generally complicate solid-state NMR spectra and increase acquisition times, they also act as a rich source of information on molecular structure and dynamics.

Several solution ^{45}Sc NMR studies have established a chemical shift range of approximately 250 ppm.[22−35] By contrast, there are few reported examples of solid-state ^{45}Sc NMR and even fewer in which chemical shielding (CS) and electric field gradient (EFG) tensor parameters have been measured. In a preliminary study by Thompson and Oldfield, the isotropic scandium chemical shift (δ_{iso}), ^{45}Sc quadrupolar coupling constant (C_Q), and the electric field gradient asymmetry parameter (η_Q) of $Sc(OAc)_3$ (OAc = acetate) and $ScCl_3 \cdot 6H_2O$ were measured.[36] Solid-state ^{45}Sc NMR was also utilized by Han et al. to observe hydrogen diffusion in hexagonally close packed scandium metal,[37] by Kataoka et al. to observe temperature-induced phase transitions in $Sc(OAc)_3$,[38] and by Koyama et al., who examined a ternary superconductor, $Sc_5Co_4Si_{10}$.[39] Several NMR studies on ferroelectric relaxors[40−43] and a variety of Sc-containing alloys and materials of mixed compositions[4,9,44,45] have also been reported. In addition, due to the favorable NMR characteristics, ^{45}Sc NMR has been employed for the design and optimization of pulse sequences for spin 7/2 nuclei.[46−48]

Chart 1

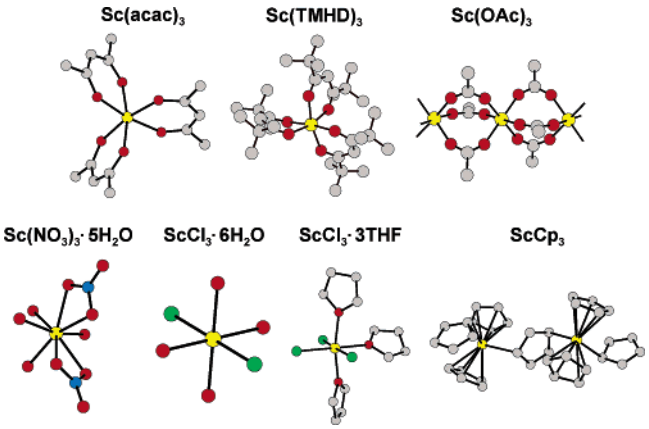

In this paper we report a comprehensive solid-state ^{45}Sc NMR study of scandium coordination complexes, in an effort to gain an understanding of the relationship between scandium coordination environments and the observed NMR parameters. The complexes under study are pictured in Chart 1 (hydrogen atoms and molecules not bound to scandium are omitted for clarity). These complexes are $Sc(acac)_3$, $Sc(TMHD)_3$, $Sc(OAc)_3$, $Sc(NO_3)_3 \cdot 5H_2O$, $ScCl_3 \cdot 6H_2O$, $ScCl_3 \cdot 3THF$, and $ScCp_3$ (acac = acetylacetonate, TMHD = 2,2,6,6-tetramethyl-3,5-heptanedionato, THF = tetrahydrofuran, and Cp = cyclopentadienyl). All of these complexes have crystal structures which were previously reported or are reported for the first time herein. These complexes were chosen because they afford a range of coordination environments about the scandium nucleus leading to the observation of an assortment of distinct CS and EFG tensor parameters. Quantum mechanical calculations of NMR interaction tensors are utilized to examine the orientation of NMR tensors within molecular frames and to help rationalize the origin of scandium NMR interactions. We also demonstrate the application of solid-state ^{45}Sc NMR for probing unknown molecular structures, including the Lewis acid catalyst $Sc(OTf)_3$ and a polystyrene microencapsulated (ME) form of $Sc(OTf)_3$ (OTf = SO_3CF_3). Application of solid-state NMR to the ME-$Sc(OTf)_3$ is of particular interest, since structural changes imparted by microencapsulation increase the catalytic activity of $Sc(OTf)_3$ in carbon−carbon bond-forming reactions.

Experimental Section

Samples of tris(cyclopentadienyl) scandium ($ScCp_3$) and scandium chloride hexahydrate ($ScCl_3 \cdot 6H_2O$) were purchased from Sigma-Aldrich Canada, Ltd., and used without further purification. A sample of scandium acetate hydrate ($Sc(OAc)_3 \cdot xH_2O$) was acquired from Sigma-Aldrich Canada, Ltd., and was recrystallized from a 5.0 M aqueous solution of acetic acid and dried in vaccuo to produce anhydrous scandium acetate ($Sc(OAc)_3$). Samples of tris(2,2,6,6-tetramethyl-3,5-heptanedionato)scandium ($Sc(TMHD)_3$), scandium nitrate pentahydrate ($Sc(NO_3)_3 \cdot 5H_2O$), scandium trifluoromethanesulfonate ($Sc(OTf)_3$), and scandium trifluoromethanesulfonate microencapsulated in a styrene polymer (ME-$Sc(OTf)_3$) were purchased from Strem Chemicals, Inc., and used without further purification. Samples of scandium tris(acetylacetonate) ($Sc(acac)_3$) and scandium chloride tris(tetrahydrofuran) ($ScCl_3 \cdot 3THF$) were synthesized in the research laboratories of Prof. Warren Piers at the University of Calgary using standard procedures.[49,50]

(22) Melson, G. A.; Olszanski, D. J.; Rahimi, A. K. *Spectrochim. Acta, Part A* **1977**, *33*, 301.
(23) Haid, E.; Kohnlein, D.; Kossler, G.; Lutz, O.; Messner, W.; Mohn, K. R.; Nothaft, G.; Vanrickelen, B.; Schich, W.; Steinhauser, N. *Z. Naturforsch., A: Phys. Sci.* **1983**, *38*, 317.
(24) Bougeard, P.; Mancini, M.; Sayer, B. G.; McGlinchey, M. J. *Inorg. Chem.* **1985**, *24*, 93.
(25) Mason, J. *Multinucl. NMR*; Plenum Press: New York, 1987; p 480.
(26) Rehder, D.; Speh, M. *Inorg. Chim. Acta* **1987**, *135*, 73.
(27) Kirakosyan, G. A.; Tarasov, V. P.; Buslaev, Y. A. *Magn. Reson. Chem.* **1989**, *27*, 103.
(28) Randarevich, S. B.; Soloveva, L. G.; Korovin, V. Y.; Nikonov, V. I.; Pastukhova, I. V. *Koord. Khim.* **1989**, *15*, 1581.
(29) Rehder, D.; Hink, K. *Inorg. Chim. Acta* **1989**, *158*, 265.
(30) Aramini, J. M.; Vogel, H. J. *J. Am. Chem. Soc.* **1994**, *116*, 1988.
(31) Miyake, Y.; Suzuki, S.; Kojima, Y.; Kikuchi, K.; Kobayashi, K.; Nagase, S.; Kainosho, M.; Achiba, Y.; Maniwa, Y.; Fisher, K. *J. Phys. Chem.* **1996**, *100*, 9579.
(32) Meehan, P. R.; Willey, G. R. *Inorg. Chim. Acta* **1999**, *284*, 71.
(33) Hill, N. J.; Levason, W.; Popham, M. C.; Reid, G.; Webster, M. *Polyhedron* **2002**, *21*, 1579.
(34) Petrosyants, S. P.; Ilyukhin, A. B. *Russ. J. Coord. Chem.* **2004**, *30*, 194.
(35) Gierezyk, B.; Schroeder, G. *Pol. J. Chem.* **2003**, *77*, 1741.
(36) Thompson, A. R.; Oldfield, E. *J. Chem. Soc., Chem. Commun.* **1987**, 27.
(37) Han, J. W.; Chang, C. T.; Torgeson, D. R.; Seymour, E. F. W.; Barnes, R. G. *Phys. Rev. B: Condens. Matter* **1987**, *36*, 615.
(38) Kataoka, H.; Takeda, S.; Nakamura, N. *J. Phys. Soc. Jpn.* **1993**, *62*, 1478.
(39) Koyama, T.; Sugita, H.; Wada, S.; Tsutsumi, K. *J. Phys. Soc. Jpn.* **1999**, *68*, 2326.
(40) Glinchuk, M. D.; Bykov, I. P.; Laguta, V. V.; Nokhrin, S. N. *Ferroelectrics* **1997**, *199*, 173.
(41) Blinc, R.; Zalar, B.; Gregorovic, A.; Pirc, R.; Glinchuk, M. D. *Ferroelectrics* **2000**, *240*, 1473.
(42) Laguta, V. V.; Glinchuk, M. D.; Nokhrin, S. N.; Bykov, I. P.; Blinc, R.; Gregorovic, A.; Zalar, B. *Phys. Rev. B: Condens. Matter* **2003**, *67*.
(43) Laguta, V. V.; Glinchuk, M. D.; Bykov, I. P.; Blinc, R.; Zalar, B. *Phys. Rev. B: Condens. Matter* **2004**, *69*, 054103.
(44) Sato, K.; Takeda, S.; Fukuda, S.; Minamisono, T.; Tanigaki, M.; Miyake, T.; Maruyama, Y.; Matsuta, K.; Fukuda, M.; Nojiri, Y. *Z. Naturforsch., A: Phys. Sci.* **1998**, *53*, 549.
(45) Tien, C.; Charnaya, E. V.; Sun, S. Y.; Wu, R. R.; Ivanov, S. N.; Khazanov, E. N. *Phys. Status Solidi B* **2002**, *233*, 222.
(46) Madhu, P. K.; Johannessen, O. G.; Pike, K. J.; Dupree, R.; Smith, M. E.; Levitt, M. H. *J. Magn. Reson.* **2003**, *163*, 310.
(47) Morais, C. M.; Lopes, M.; Fernandez, C.; Rocha, J. *Magn. Reson. Chem.* **2003**, *41*, 679.
(48) Brauniger, T.; Ramaswamy, K.; Madhu, P. K. *Chem. Phys. Lett.* **2004**, *383*, 403.
(49) Atwood, J. L.; Smith, K. D. *J. Chem. Soc., Dalton Trans.* **1974**, 921.

Table 1. Summary of Observed ^{45}Sc EFG and CS Tensor Parameters[a]

compound	C_Q (MHz)[b]	η_Q[c]	δ_{iso} (ppm)[d]	Ω (ppm)[e]	κ[f]	α (deg)	β (deg)	γ (deg)
$Sc(acac)_3$	13.0(3)[g]	0.22(3)	82(1)	70(10)	−0.7(2)	90(15)	83(4)	0(5)
$Sc(TMHD)_3$	13.1(2)	0.93(2)	89.5(10)	110(20)	−0.7(3)	0(10)	15(15)	90(5)
$Sc(NO_3)_3{\cdot}5H_2O$	6.2(2)	0.75(5)	−18.5(10)	60(10)	−0.8(1)	80(15)	10(10)	65(15)
$Sc(OAc)_3$	4.6(2)	0.18(6)	−6.2(8)	73(5)	0.65(10)	0(45)	7(3)	90(45)
$ScCl_3{\cdot}6H_2O$	3.9(2)	0.77(9)	125.4(5)	180(10)	0.9(1)	45(10)	30(5)	40(10)
$ScCl_3{\cdot}3THF$	8.4(2)	0.30(5)	202(1)	200(20)	−0.1(3)	85(35)	4(4)	12(25)
Cp_3Sc	8.3(2)	0.88(4)	62.8(8)	135(15)	0.0(3)	−24(10)	73(8)	130(15)

[a] The CS tensor is described by three principal components ordered such that $\sigma_{11} \le \sigma_{22} \le \sigma_{33}$. The EFG tensor is described by three principal components ordered such that $|V_{11}| \le |V_{22}| \le |V_{33}|$. [b] $C_Q = eQV_{33}/h$. [c] $\eta_Q = (V_{11} - V_{22})/V_{33}$. [d] $\delta_{jj} = (\sigma_{iso,ref} - \sigma_{jj})(10^6)/(1 - \sigma_{iso,ref}) \approx \sigma_{iso,ref} - \sigma_{jj}$, where jj = 11, 22, or 33, $\delta_{iso} = (\delta_{11} + \delta_{22} + \delta_{33})/3$. [e] $\Omega = \delta_{11} - \delta_{33}$. [f] $\kappa = 3(\delta_{22} - \delta_{iso})/\Omega$. [g] The uncertainty in the last digits of each value is denoted in parentheses.

A second sample of $ScCl_3{\cdot}3THF$ was prepared by adding anhydrous $ScCl_3$ to an excess of THF. The sample was then dried in vaccuo and used without further purification. All samples were finely ground, packed into 4 mm outer diameter zirconia rotors and sealed with airtight caps under a nitrogen or argon atmosphere. The $Sc(acac)_3$ and $Sc(TMHD)_3$ samples were prepared in a similar manner outside of the glovebox.

Solid-state ^{45}Sc, ^{13}C, and ^{19}F NMR spectra were acquired on a Varian Infinity Plus spectrometer with an Oxford 9.4 T ($\nu_0(^1H)$ = 400 MHz) wide-bore magnet. Additional ^{45}Sc static spectra were acquired on a Bruker Avance 500 spectrometer with an 11.75 T ($\nu_0(^1H)$ = 500 MHz) magnet. ^{45}Sc chemical shifts were reported with respect to an external standard solution of 0.11 m (mol of solute/kg of solvent) $ScCl_3$ in 0.05 M HCl (δ_{iso} = 0.0 ppm). As there is currently no universally applied scandium NMR standard, this sample was chosen due to the sharp peak observed in its solution NMR spectrum, and the insensitivity of the scandium chemical shift to changes in hydrogen chloride concentrations from 0.05 to 1.0 M.[23] ^{13}C chemical shifts were referenced to tetramethylsilane (δ_{iso} = 0.0 ppm) by using the high-frequency peak of adamantane as a secondary reference (δ_{iso} = 38.57 ppm). ^{19}F chemical shifts were referenced to fluorotrichloromethane (δ_{iso} = 0.0 ppm) by setting the ^{19}F resonance of Teflon (δ_{iso} = −122.0 ppm) as a secondary reference.

Central-transition selective $\pi/2$ pulse widths were calculated by scaling the nonselective pulses by a factor of a quarter, i.e., $(I + 1/2)^{-1}$. Unless otherwise noted, the Hahn-echo pulse sequence of the form $\{\pi/2-\tau-\pi-\tau-\text{acquire}\}$ was used for the acquisition of ^{45}Sc NMR spectra. Static ^{45}Sc NMR spectra of $Sc(acac)_3$, $Sc(OAc)_3$, and $ScCl_3{\cdot}3THF$ were also acquired with an echo pulse sequence of the form $\{\pi/2-\tau-\pi/2-\tau-\text{acquire}\}$ (90−90 echo). Rotary-assisted polarization transfer (RAPT)[51] and amplitude-modulated double frequency sweep (AM-DFS)[52] pulse sequences were employed for the acquisition of selected spectra. ^{45}Sc NMR experiments were conducted at $\nu_0(^{45}Sc)$ = 97.4 MHz (9.4 T) and 122.0 MHz (11.75 T). The rf fields used for acquisition of the static ^{45}Sc NMR spectra were generally set to half of the pattern width to avoid line shape distortions.[53] All experimental parameters can be found in Table S1 (Supporting Information). Analytical simulations of ^{45}Sc solid-state NMR spectra were performed using WSolids,[54] and numerical simulations were performed using SIMPSON.[55]

^{13}C NMR spectra were acquired using Hahn-echo and variable-amplitude cross- polarization MAS (VACP/MAS) pulse sequences. $^1H \rightarrow {}^{13}C$ CP was performed on all samples for the acquisition of ^{13}C spectra, except for the $Sc(OTf)_3$ samples, for which $^{19}F \rightarrow {}^{13}C$ CP was applied. The TPPM[56] decoupling sequence was employed in all cases. Solid-state ^{19}F NMR spectra were acquired with a rotor-synchronized Hahn-echo pulse sequence. All ^{13}C and ^{19}F NMR data are presented in the Supporting Information.

Calculations of CS and EFG tensors were performed using Gaussian 03[57] running on two Dell Precision workstation running Red Hat Linux 9.0. Molecular coordinates were input from structures determined by single-crystal X-ray diffraction experiments, and proton positions were geometry-optimized for most structures. Calculations were carried out using restricted Hartree−Fock (RHF) and hybrid density functional theory (DFT) employing the B3LYP functional.[58] The basis sets 6-31G**, 6-31+G**, 6-311G**, and 6-311+G** were used for all calculations. All-electron basis sets on scandium were also employed for calculations on $Sc(acac)_3$.[59] CS tensors were calculated using the gauge-including atomic orbitals (GIAO) method.[60,61] $[Sc(H_2O)_6]^{3+}$ was chosen to model the chemical shielding of the solution standard,[62] and absolute shieldings were converted to shifts as described in Tables 1 and 2.

Suitable single crystals of $ScCl_3{\cdot}6H_2O$ and $Sc(NO_3)_3{\cdot}5H_2O$ were selected for X-ray diffraction experiments from the purchased samples and used without recrystallization. $Sc(TMHD)_3$ was recrystallized in dichloromethane. All crystals were coated in Nujol oil to prevent the absorption of water. Diffraction experiments were performed on a Siemens SMART System CCD diffractometer. The data were processed using the SAINT+ software package,[63] and an absorption correction was applied to the data using SADABS. The structure was solved by direct methods and refined by full-matrix least-squares against F^2 using the SHELXTL software package.[64] For experimental parameters refer to Table S2.

Powdered $ScCl_3{\cdot}3THF$, $Sc(OAc)_3$, and $Sc(OTf)_3$ were packed into 1.0 mm glass capillary tubes under nitrogen and flame sealed. Powder X-ray diffraction patterns were collected using a Bruker AXS HI-STAR system using a general area detector diffractions system. The X-ray source employed was Cu Kα radiation (1.540598 Å) with an area detector using a 2θ range between 4.0 and 65.0°. Powder X-ray diffraction patterns were simulated with the Powder Cell software package.[65]

Results and Discussion

In the first part of this section, a detailed discussion of ^{45}Sc NMR spectroscopy of scandium coordination compounds is presented. In all of the cases discussed herein, it is possible to utilize MAS to almost completely average the scandium CSA,

(50) Morgan, G. T.; Moss, H. W. *J. Chem. Soc., Trans.* **1914**, 189.
(51) Yao, Z.; Kwak, H. T.; Sakellariou, D.; Emsley, L.; Grandinetti, P. J. *Chem. Phys. Lett.* **2000**, *327*, 85.
(52) Kentgens, A. P. M.; Verhagen, R. *Chem. Phys. Lett.* **1999**, *300*, 435.
(53) Bodart, P. R.; Amoureux, J. P.; Dumazy, Y.; Lefort, R. *Mol. Phys.* **2000**, *98*, 1545.
(54) Eichele, K.; Wasylishen, R. E. WSolids1: Solid-State NMR Spectrum Simulation, v. 1.17.30, 2001.
(55) Bak, M.; Rasmussen, J. T.; Nielsen, N. C. *J. Magn. Reson.* **2000**, *147*, 296.
(56) Bennett, A. E.; Rienstra, C. M.; Auger, M.; Lakshmi, K. V.; Griffin, R. G. *J. Chem. Phys.* **1995**, *103*, 6951.
(57) Frisch, M. J. *Gaussian 03*, rev. B.03; Gaussian, Inc.: Pittsburgh, PA, 2003.
(58) Lee, C.; Yang, W.; Parr, R. G. *Phys. Rev. B: Condens. Matter* **1988**, *37*, 785.
(59) Huzinaga, S., Ed. *Gaussian Basis Sets for Molecular Calculations*; Elsevier: New York, 1984.
(60) Wolinski, K.; Hinton, J. F.; Pulay, P. *J. Am. Chem. Soc.* **1990**, *112*, 8251.
(61) Ditchfield, R. *Mol. Phys.* **1974**, *27*, 789.
(62) Rudolph, W. W.; Pye, C. C. *J. Phys. Chem. A* **2000**, *104*, 1627.
(63) *Bruker SAINT+*, v. 6.45; Bruker AXS Inc.: Madison, WI, 2003.
(64) Sheldrick, G. M. *SHELXTL*, v. 6.10; Bruker AXS Inc.: Madison, WI, 2000.
(65) Kraus, W.; Nolze, G. *PowderCell for Windows*, v. 2.4; Federal Institute for Materials Research and Testing: Berlin, Germany, 2000.

Table 2. Calculated ^{45}Sc NMR Parameters Showing Best Agreement with Experiment[a]

compound/method	C_Q (MHz)[b]	η_Q	δ_{iso} (ppm)[c]	Ω (ppm)	κ	α (deg)	β (deg)	γ (deg)
Sc(acac)$_3$[d]	13.0(3)	0.22(3)	82(1)	70(10)	−0.7(2)	90(15)	83(4)	0(5)
RHF/6-311G** on Sc[e]	−11.6	0.44	77.0	61.3	−0.69	89	85	1
B3LYP/6-311G**	−12.3	0.40	101.8	95.1	−0.67	85	85	2
Sc(TMHD)$_3$	13.1(2)	0.93(2)	89.5(10)	110(20)	−0.7(3)	0(10)	15(15)	90(5)
RHF/6-311+G** on Sc	14.4	0.67	76.1	82.5	0.57	90	68	0
B3LYP/6-311G** on Sc	15.3	0.71	98.4	118.8	0.36	90	5	0
Sc(NO$_3$)$_3$·5H$_2$O	6.2(2)	0.75(5)	−18.5(10)	60(10)	−0.8(1)	80(15)	10(10)	65(15)
RHF/6-311G**	−5.6	0.72	7.3	58.9	−0.74	51	39	75
B3LYP/6-311+G**	−5.8	0.96	46.4	70.9	0.20	25	33	89
Sc(OAc)$_3$	4.6(2)	0.18(6)	−6.2(8)	73(5)	0.65(10)	0(45)	7(3)	90(45)
RHF/6-311G**	3.3	0.18	15.8	24.9	0.86	1	6	90
B3LYP/6-311G**	4.6	0.00	−19.4	102.6	0.99	0	0	90
ScCl$_3$·6H$_2$O	3.9(2)	0.77(9)	125.4(5)	180(10)	0.9(1)	45(10)	30(5)	40(10)
RHF/6-311G** on Sc	5.3	0.78	154.4	228.9	0.96	51	26	40
B3LYP/6-311+G** on Sc	5.3	0.74	231.3	486.2	0.98	52	25	38
ScCl$_3$·3THF	8.4(2)	0.30(5)	202(1)	200(20)	−0.1(3)	85(35)	4(4)	12(25)
RHF/6-311G** on Sc	9.7	0.26	176.8	157.8	−0.11	80	5	12
B3LYP/6-311G**	10.0	0.35	303.0	316.7	−0.26	73	4	18
ScCp$_3$	8.3(2)	0.88(4)	62.8(8)	135(15)	0.0(3)	−24(10)	73(8)	130(15)
RHF/6-311G** on Sc	−8.5	0.90	−74.6	86.1	−0.02	60	43	20
B3LYP/6-311+G** on Sc	−7.9	0.74	115.1	300.5	−0.34	−47	36	36

[a] All computational results can be found in Table S4. [b] Only the magnitude of C_Q can be measured experimentally. For definitions of all NMR parameters refer to Table 1. [c] The theoretical isotropic shifts were calculated by comparison of the calculated shielding to that calculated from a geometry-optimized model of $[Sc(H_2O)_6]^{3+}$ at the appropriate level of theory. [d] Experimental results from this paper. [e] In cases where the basis set used for scandium is explicitly stated the 6-31G** basis set was employed on all other atoms.

while partially averaging the second-order QI. Therefore, the values of C_Q, η_Q, and δ_{iso} can be readily obtained by analytical simulations of the ^{45}Sc MAS NMR central transition spectra (Table 1). Static ^{45}Sc NMR spectra allow for the measurement of both quadrupolar (C_Q and η_Q) and CS tensor parameters (δ_{iso}, as well as the span, Ω, and the skew, κ), as well as the Euler angles (α, β, and γ) which describe the relative orientation of EFG and CS tensors (see Table 1 for definitions of these parameters). Static spectra acquired at a second field are used to confirm the observed CS tensor parameters and Euler angles.[66,67] The shapes of the static powder patterns are sensitive to the pulse sequences and rf fields used in their acquisition (Figure S1); fortunately, the locations of discontinuities, which are paramount for determination of spectral parameters, are largely unaffected by these factors. To the best of our knowledge, there are no previous reports of scandium CSA in the literature. Spectral simulations presented throughout the paper account for scandium CSA; for comparison, spectral simulations that neglect the presence of CSA are found in the Supporting Information (Figure S2). In the second part of this section, theoretically calculated CS and EFG tensors and their orientations and origins are investigated in depth. In the final part of this section, we examine the application of ^{45}Sc NMR to structurally characterize systems for which crystallographic and/or other structural data are unavailable. Details on newly determined crystal structures are found in the Supporting Information.

Solid-State ^{45}Sc NMR Experiments. Sc(acac)$_3$. The solid-state ^{45}Sc MAS NMR spectrum of the central transition (Figure 1a) is simulated with $C_Q = 13.0$ MHz, $\eta_Q = 0.22$, and $\delta_{iso} = 82$ ppm. Experimental and simulated static ^{45}Sc NMR spectra of Sc(acac)$_3$ acquired at two different magnetic field strengths (Figure 1b) reveal that $\Omega = 70$ ppm and $\kappa = -0.7$ (all Euler angles are tabulated in Table 1). The "shoulder" on the low-frequency side of the MAS spectrum is not predicted by the analytical simulation; however, a numerical simulation using SIMPSON reveals that this shoulder is due to the presence of an underlying satellite transition (Figure 1a, inset).

The nature of the EFG and CS tensors and their relation to one another as well as the molecular frame can be rationalized by considering the molecular structure. The scandium atom is coordinated by six oxygen atoms from the three bidentate acetylacetonato ligands.[68] Inspection of the crystal structure reveals that the coordination sphere formed by the oxygen atoms more closely resembles a trigonal antiprism and deviates considerably from octahedral geometry (and therefore spherical symmetry).[2] There are only minor variations in the Sc−O bond lengths (~0.02 Å); however, deviations of up to 10° from ideal octahedral angles are observed in the O−Sc−O bond angles. In this respect, the observation of a relatively large C_Q is not surprising (this is the second largest value of C_Q observed in this series of complexes). The value of η_Q is closer to zero than one, indicating that V_{33} is the pseudo-unique component of the EFG tensor. The appreciable span indicates that the scandium chemical shielding is anisotropic, and the skew indicates that σ_{11} is the pseudo-unique component (i.e., the values of σ_{22} and σ_{33} are closer to one another than σ_{11} and σ_{22}). The Euler angles indicate that the largest component of the EFG tensor which defines the magnitude of the quadrupolar interaction, V_{33}, is nearly coincident with σ_{11}, the principal component of the CS tensor which describes the direction of least magnetic shielding. Given the near-axial symmetry of each tensor, one would expect that V_{33} and σ_{11} are aligned near the pseudo-threefold axis of the molecule. Proposed tensor orientations are investigated further in the discussion of ab initio calculations for this molecule and all remaining systems.

Sc(TMHD)$_3$. Simulation of the ^{45}Sc MAS NMR spectrum of Sc(TMHD)$_3$ (Figure 1c) reveals $C_Q = 13.1$ MHz and $\delta_{iso} = 89.5$ ppm. Simulation of the static ^{45}Sc NMR spectra (Figure

(66) Cheng, J. T.; Edwards, J. C.; Ellis, P. D. *J. Phys. Chem.* **1990**, *94*, 553.
(67) Power, W. P.; Wasylishen, R. E.; Mooibroek, S.; Pettitt, B. A.; Danchura, W. *J. Phys. Chem.* **1990**, *94*, 591.
(68) Anderson, T. J.; Neuman, M. A.; Gordon, A. M. *Inorg. Chem.* **1973**, *12*, 927.

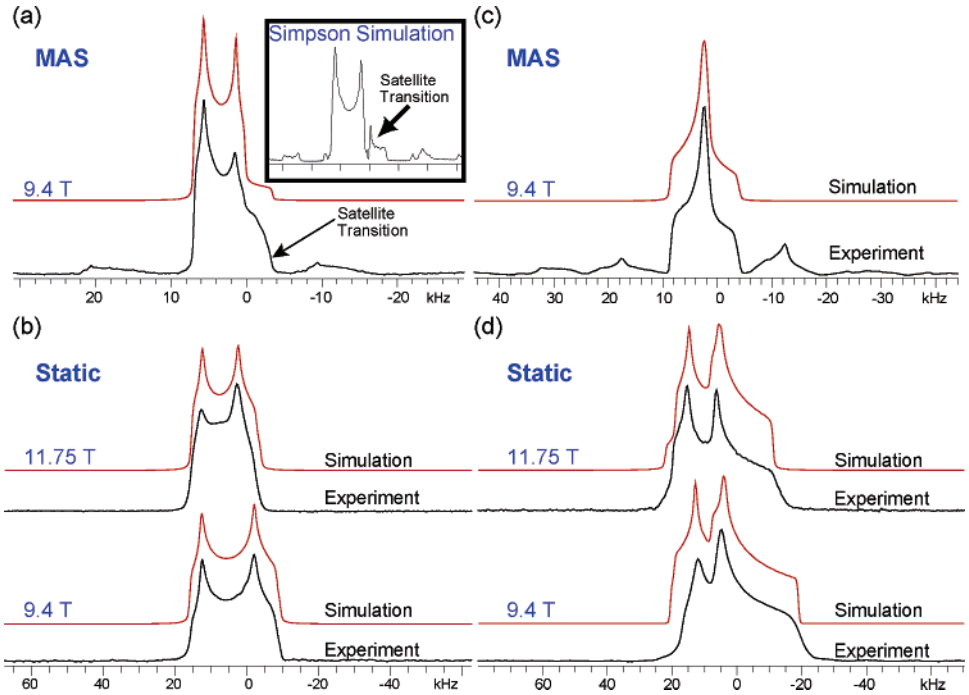

Figure 1. Solid-state ^{45}Sc NMR spectra and analytical simulations of $Sc(acac)_3$ and $Sc(TMHD)_3$. (a) MAS spectrum of $Sc(acac)_3$, $\nu_{rot} = 15$ kHz. Inset: SIMPSON simulation utilizing ideal pulses and processed with 100 Hz of exponential line broadening. (b) Static spectra of $Sc(acac)_3$ at 9.4 and 11.75 T. The static spectrum at 9.4 T was acquired with a 90−90 echo. (c) MAS RAPT-echo spectrum of $Sc(TMHD)_3$, $\nu_{rot} = 15$ kHz. (d) Static spectra of $Sc(TMHD)_3$ at 9.4 and 11.75 T.

1d) yield parameters similar to those observed in $Sc(acac)_3$, with $\Omega = 110$ ppm and $\kappa = -0.7$; however, the Euler angles are different. The ligands and their coordination to Sc in $Sc(acac)_3$ and $Sc(TMHD)_3$ are analogous, so that the observation of similar values of δ_{iso} and C_Q are not surprising. However, $\eta_Q = 0.93$, which indicates that V_{11} is the most distinct component of the EFG tensor and is oriented along or near the 2-fold molecular axis, in contrast to $Sc(acac)_3$. The difference in relative tensor orientations between the two complexes can be explained by comparison of the crystal structures. In $Sc(acac)_3$, each of the ligands forms an approximately planar six-membered ring with the scandium center; however, in $Sc(TMHD)_3$, there is a 22° deviation away from planarity in two of the three six-membered rings. The molecule is now more properly described as possessing C_2 symmetry, and this difference in symmetry is the major cause of the distinct EFG tensor orientation. The low value of β also means that V_{33} and σ_{33} are closely oriented, unlike in $Sc(acac)_3$. Thus, changes in the geometry of the ligand at a distance from the scandium center have dramatically affected the relative orientation of the EFG and CS tensors.

$Sc(NO_3)_3{\cdot}5H_2O$. The ^{45}Sc MAS NMR spectrum of $Sc(NO_3)_3{\cdot}5H_2O$ (Figure 2a) reveals a much narrower powder pattern than those observed for the diketonato compounds. From the MAS and static spectra (Figure 2b) the measured parameters are $C_Q = 6.2$ MHz, $\eta_Q = 0.75$, $\delta_{iso} = -18.5$ ppm, $\Omega = 60$ ppm, and $\kappa = -0.8$. The ^{45}Sc nucleus is highly shielded in comparison to the distorted octahedral environments discussed above, and a relatively small scandium CSA is also observed. The observation of a relatively small C_Q is unexpected, given the considerably nonspherical coordination environment about scandium that is revealed in the single-crystal X-ray structure (details in Table S2). However, inspection of the Sc−O bond lengths reveals that they are longer than those observed in $Sc(acac)_3$ and $Sc(OAc)_3$ (the Sc−O bonds of water and the nitrate ligands are on average 0.14 and 0.21 Å longer, respectively). The decreased EFG must therefore result from the increased Sc−O bond distances. Similar observations have been made in numerous systems where increased bond lengths and augmented ionic character tend to result in lowering of C_Q, since the magnitude of V_{33} is proportional to $1/r^3$ in a simple point charge model.[69,70]

$Sc(OAc)_3$. MAS and static ^{45}Sc NMR spectra of $Sc(OAc)_3$ reveal a relatively narrow central transition (Figure 2c,d), and simulations yield $C_Q = 4.6$ MHz, $\eta_Q = 0.18$, $\delta_{iso} = -6.2$ ppm, $\Omega = 73$ ppm, and $\kappa = 0.65$. Solid-state ^{45}Sc NMR spectra of $Sc(OAc)_3$ have been reported previously by Thompson and Oldfield, as well as Kataoka et al. Both groups reported $C_Q = 5$ MHz and $\eta_Q = 0$ from simulations of static central transition spectra.[36,38] Kataoka reported a refined $C_Q = 4.45$ MHz on the basis of a simulation of satellite transitions, which is closer to our result. In both papers, the effects of CSA were neglected in the simulations and η_Q was assumed to be zero. From the appearance of our static spectra, it is apparent that scandium CSA is present and the EFG tensor is nonaxial. These factors must be accounted for to properly simulate the static spectra.

The previously determined X-ray crystal structure[71] reveals a coordination polymer structure, with a unique Sc atom in a six-coordinate environment that results from bridging acetate ligands (our own powder XRD pattern (Figure S3) confirms that recrystallization successfully produced anhydrous $Sc(OAc)_3$). The Sc−O bond lengths are similar to those in $Sc(acac)_3$; however, the $Sc(acac)_3$ metal environment is nearly octahedral, with all *trans*-O−Sc−O bond angles equal to 180°

(69) Lucken, E. A. C. *Nuclear Quadrupole Coupling Constants*; Academic: New York, 1969.
(70) Cohen, M. H.; Reif, F. *Solid State Phys.* **1957**, *5*, 321.
(71) Fuchs, R.; Strahle, J. *Z. Naturforsch., B: Chem. Sci.* **1984**, *39*, 1662.

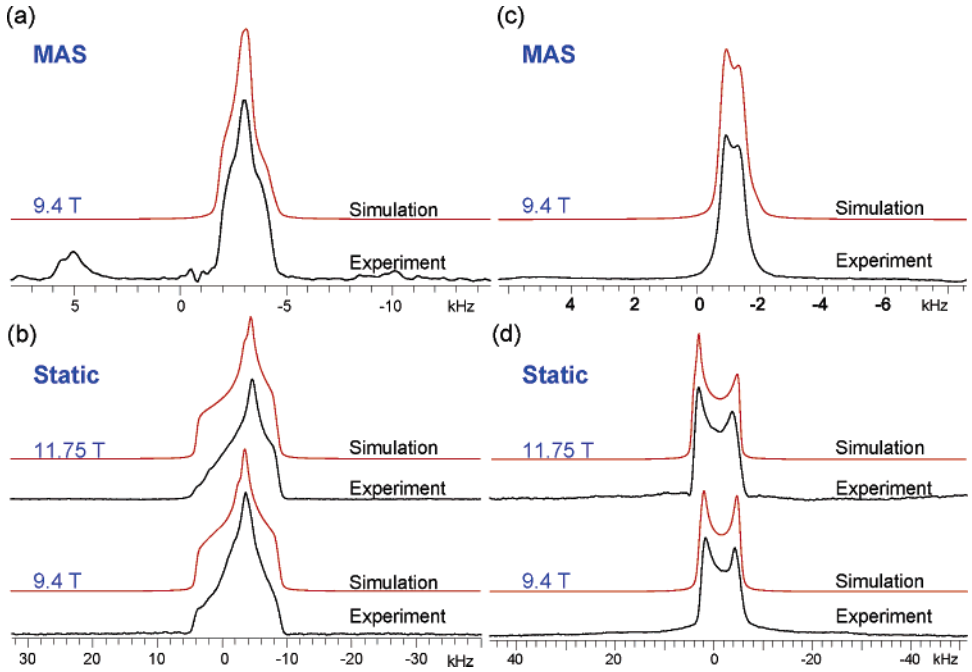

Figure 2. Solid-state ^{45}Sc NMR spectra and analytical simulations of $Sc(NO_3)_3{\cdot}5H_2O$ and $Sc(OAc)_3$: (a) MAS spectrum of $Sc(NO_3)_3{\cdot}5H_2O$, $\nu_{rot} = 8$ kHz; (b) static spectra of $Sc(NO_3)_3{\cdot}5H_2O$ at 9.4 and 11.75 T; (c) MAS spectrum of $Sc(OAc)_3$, $\nu_{rot} = 8$ kHz; (d) static spectra of $Sc(OAc)_3$ at 9.4 and 11.75 T acquired with a 90−90 echo.

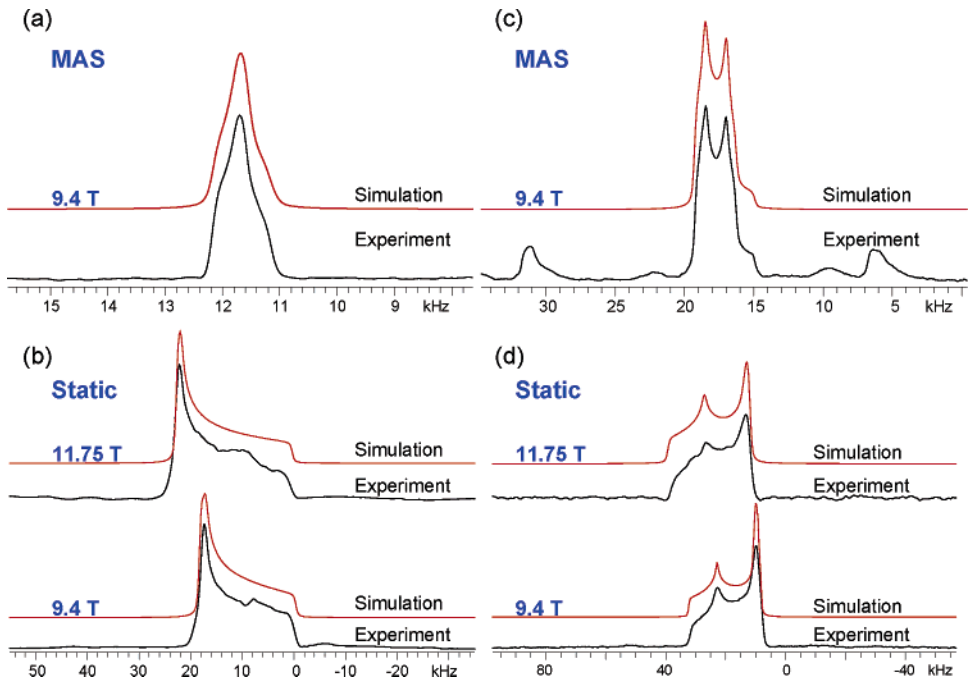

Figure 3. Solid-state ^{45}Sc NMR spectra and analytical simulations of $ScCl_3{\cdot}6H_2O$ and $ScCl_3{\cdot}3THF$: (a) MAS spectrum of $ScCl_3{\cdot}6H_2O$, $\nu_{rot} = 10$ kHz; (b) static spectra of $ScCl_3{\cdot}6H_2O$ at 9.4 and 11.75 T; (c) MAS spectrum of recrystallized $ScCl_3{\cdot}3THF$, $\nu_{rot} = 12.5$ kHz; (d) static spectra of recrystallized $ScCl_3{\cdot}3THF$ at 9.4 and 11.75 T acquired with a 90−90 echo.

and *cis*-O−Sc−O bond angles deviating only slightly from 90° (±3.5°). The relatively small C_Q can be accounted for by the nearly spherically symmetric arrangement of oxygen atoms about the scandium. The δ_{iso} and Ω values are similar to those of $Sc(NO_3)_3{\cdot}5H_2O$, but the ^{45}Sc nucleus is relatively shielded from the external magnetic field compared to those in $Sc(acac)_3$ and $Sc(TMHD)_3$, which have distorted octahedral oxygen coordination environments. The symmetry of both the CS and EFG tensors is quite distinct from that of $Sc(NO_3)_3{\cdot}5H_2O$, which is to be expected given their structural differences. The value of η_Q for $Sc(OAc)_3$ indicates that V_{33} is the distinct component of the EFG tensor, and κ indicates that σ_{33} is the unique component of the CS tensor. The low value of β indicates that V_{33} and σ_{33} are nearly collinear and are likely directed along the C_3 axis of the molecule, in the direction of propagation of the polymer structure.

$ScCl_3{\cdot}6H_2O$. The ^{45}Sc MAS NMR spectrum of $ScCl_3{\cdot}6H_2O$ (Figure 3a) reveals a very narrow powder pattern with a breadth of ca. 1 kHz, with $C_Q = 3.9$ MHz, $\eta_Q = 0.77$, and $\delta_{iso} = 125.4$ ppm. Static spectra (Figure 3b) reveal a large span, $\Omega = 180$

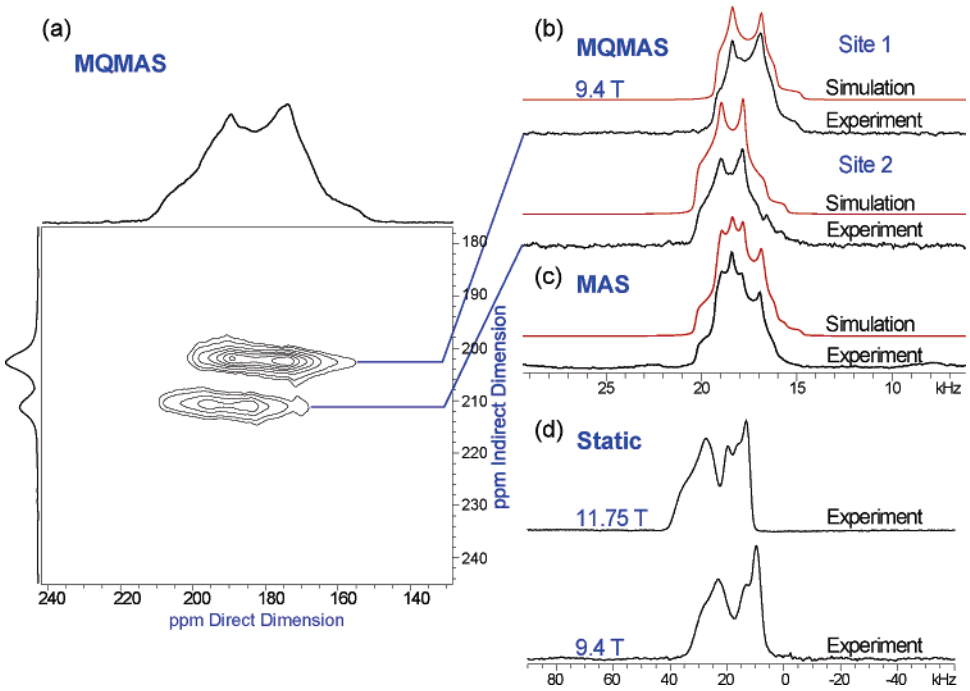

Figure 4. Solid-state ^{45}Sc NMR spectra of $ScCl_3$·3THF (first sample): (a) MQMAS contour plot, $\nu_{rot} = 8$ kHz; (b) two resolved sites from cross sections of the indirect dimension and analytical simulations; (c) MAS spectrum ($\nu_{rot} = 15$ kHz) and the simulated pattern that results from addition of the individually simulated patterns; (d) static spectra.

ppm, and a nearly axial CS tensor, $\kappa = 0.9$. The static spectra contain a distortion that is unaccounted for in the line shape of the static simulations at both fields, which likely arises from a small amount of impurity, as opposed to incomplete excitation or intramolecular dynamics. The EFG parameters for $ScCl_3$·$6H_2O$ are different from those reported by Thompson and Oldfield,[36] who found that $C_Q = 14$ MHz and $\eta_Q = 0.60$, on the basis of the acquisition and simulation of a static ^{45}Sc NMR spectrum. The differences in their parameters from ours could arise from their neglect of scandium CSA and the absence of ^{45}Sc MAS NMR data. It is also unclear whether proton decoupling was applied in their NMR experiments, which has adverse effects on the appearance of the ^{45}Sc static NMR powder pattern in this case (Figure S4).

This complex possesses the smallest observed C_Q and largest Ω in the series of compounds studied herein. These two observations can be rationalized in terms of molecular structure. The crystal structure for $ScCl_3$·$6H_2O$ was not previously reported, and our initial assumption was that the scandium atom would be coordinated by six oxygen atoms. While this structural model is consistent with the quadrupolar data, it is inconsistent with the high isotropic shift and large span. Refinement of the crystal structure of $ScCl_3$·$6H_2O$ reveals a highly symmetrical coordination environment about scandium, involving two Cl and four O atoms which form a $[ScCl_2(H_2O)_4]^+$ unit of approximately D_{4h} symmetry. The two Sc−Cl distances are equivalent and the angle separating them is 180.0°, while there is less than 1.0° deviation from ideal octahedral O−Sc−O angles. In this respect, the observations of a relatively small C_Q and large scandium CSA is not surprising. The large span and axially symmetric skew indicate that σ_{33} is likely oriented near the Sc−Cl bond axis, and that there are large paramagnetic deshielding contributions perpendicular to this axis.

$ScCl_3$·3THF. ^{45}Sc NMR spectra were acquired from two different samples of $ScCl_3$·3THF (Figures 3 and 4). Initial ^{45}Sc MAS NMR spectra acquired from this compound revealed the presence of two distinct scandium sites. A ^{45}Sc multiple-quantum MAS (MQMAS) NMR experiment[72] was performed to resolve the overlapping sites (Figure 4a), with simulations (Figure 4b) yielding $C_Q = 8.5$ MHz, $\eta_Q = 0.32$, and $\delta_{iso} = 201.5$ ppm (site 1) and $C_Q = 8.5$ MHz, $\eta_Q = 0.50$, and $\delta_{iso} = 211.0$ ppm (site 2). Simulated spectra are coadded to simulate the observed MAS spectra (Figure 4c). The overlapping static powder patterns render determination of the CS tensor parameters and Euler angles difficult (Figure 4d).

The observation of two scandium sites in the NMR spectra was surprising because the previously reported crystal structure indicates that only one crystallographically and magnetically distinct Sc site should be present.[49] The powder XRD pattern (Figure S3) indicates that this sample is highly crystalline, though additional high intensity peaks indicate that there is a second species or crystalline phase present. The presence of impurities in this sample is unlikely, given the roughly equal NMR signal intensities and the similar NMR parameters of the two scandium sites. Recrystallization of anhydrous $ScCl_3$ in an excess of THF was performed. NMR spectra acquired from this second sample yielded one scandium resonance as expected (Figure 3c,d), and spectra are simulated with $C_Q = 8.4$ MHz, $\eta_Q = 0.30$, $\delta_{iso} = 202$ ppm, $\Omega = 200$ ppm, and $\kappa = -0.1$. The powder XRD pattern of the recrystallized sample closely matches the predicted pattern. Clearly, the combination of ^{45}Sc MQMAS NMR and powder XRD is extremely useful for differentiating Sc sites in similar coordination environments.

$ScCl_3$·3THF consists of a scandium atom coordinated by three chlorine atoms and three THF molecules in a meridional fashion. The large positive chemical shift (the highest in this series) and large span are consistent with the notion that replacement of an oxygen with chlorine in the first coordination sphere results

(72) Medek, A.; Harwood: J. S.; Frydman, L. *J. Am. Chem. Soc.* **1995**, *117*, 12779.

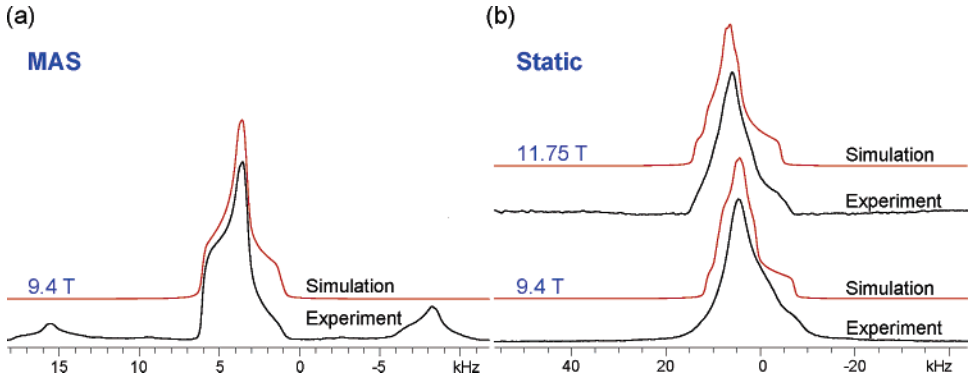

Figure 5. Solid-state ^{45}Sc NMR spectra of $ScCp_3$ and simulations: (a) MAS spectrum, $\nu_{rot} = 12$ kHz; (b) static spectra at 9.4 and 11.75 T.

in magnetic deshielding of the scandium nucleus. The Sc−Cl bonds are considerably more covalent than Sc−O bonds; as such, there are increased paramagnetic shielding contributions perpendicular to the Sc−Cl bond axes. Given the meridional arrangement of Cl and O atoms, σ_{11} should be oriented in a direction perpendicular to all three Sc−Cl bonds. The nonaxial κ indicates that the CS tensor does not have a pseudo-unique component. The skew, the moderate value of C_Q, and the nonaxial η_Q are all consistent with the meridional arrangement of Cl and O atoms in the in the first coordination sphere.

$ScCp_3$. This compound represents a departure from all other systems studied herein and is mentioned as an aside. Given current interest in organometallic scandium compounds,[18−21] solid-state ^{45}Sc NMR could be a useful method to gain insight into their molecular structure and dynamics. In this regard, $ScCp_3$ is a good entry point for studies upon π-coordinated systems. Herein we present some preliminary room-temperature NMR data. Analytical simulation of ^{45}Sc MAS (Figure 5a) and static (Figure 5b) NMR spectra of $ScCp_3$ yield $\delta_{iso} = 62.8$ ppm, $C_Q = 8.3$ MHz, $\eta_Q = 0.88$, $\Omega = 135$ ppm, and $\kappa = 0.0$. The discontinuities in static spectra are difficult to resolve at both 9.4 and 11.75 T, increasing the errors in the CS tensor parameters and Euler angles. The appearance of the spectra are suggestive of some intramolecular dynamics, though this is beyond the scope of the current paper (see ^{13}C NMR data in Figure S6).

The structure of $ScCp_3$ consists of two η^5-Cp rings and two η^1-Cp rings. The η^1-Cp rings bridge two adjacent scandium atoms leading to the formation of polymeric chains. In the majority of NMR studies of metal nuclei in metallocene systems,[73−77] the values of δ_{iso} typically occur far to the low-frequency end of the chemical shift range, consistent with nuclei which are highly shielded from the magnetic field. In this respect, the "midrange" δ_{iso} for this metallocene system is unusual. The η^5-Cp rings are likely responsible for significant magnetic shielding of the ^{45}Sc nucleus, while η^1-Cp must result in some degree of deshielding. With the absence of other organometallic species for comparison, it is difficult to assess the origin of the moderate value of C_Q, though this will be the subject of a future study.

Summary of Observed ^{45}Sc NMR Parameters. To aid in illustrating the observed trends, a chemical shift scale has been

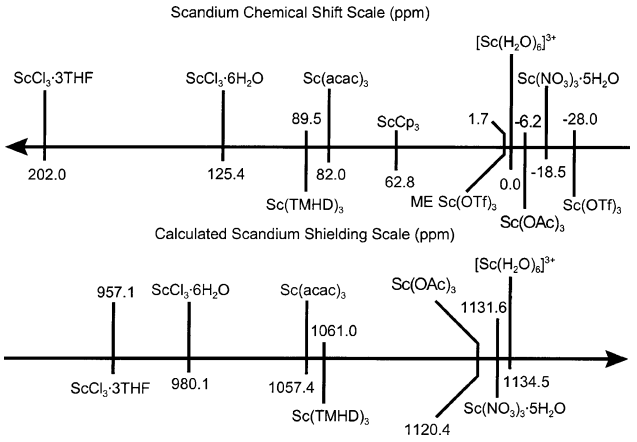

Figure 6. ^{45}Sc chemical shift and shielding scales. The chemical shielding scale was generated from the RHF/6-311G** on Sc series of calculations. The theoretical result for $ScCp_3$ has been omitted.

constructed from all of the complexes studied herein (Figure 6). Magnetic deshielding is observed upon replacement of oxygen with chlorine; for instance, the isotropic chemical shift of scandium in $ScCl_3{\cdot}6H_2O$ is 125.4 ppm (coordination by two chlorine atoms), while the observed shift of $ScCl_3{\cdot}3THF$ is 202 ppm (coordination by three chlorine atoms). Sc−Cl bonding must play a significant role in making paramagnetic shielding contributions and increasing the span of the scandium CS tensors. A trend in the observed values of Ω is also observed: coordination of scandium by more than one type of atom or by ligands engaging in multiple binding modes (e.g. $ScCp_3$) is seen to result in sizable Ω values.

A correlation between molecular symmetry and size of C_Q is also observed. A C_Q of 2.02 MHz in hexagonally closed packed Sc metal has been previously observed,[37] which is reflective of the spherically symmetric scandium environment. Compounds that possess coordination environments with bond angles close to ideal octahedral angles, such as $Sc(OAc)_3$ and $ScCl_3{\cdot}6H_2O$, are seen to possess relatively small values of C_Q. Distortions away from octahedral symmetry result in an increase in C_Q as observed in $Sc(acac)_3$ and $Sc(TMHD)_3$. Values of η_Q near zero or one are observed when symmetry elements such as rotational axes are present.

The aforementioned trends illustrate the utility of solid-state ^{45}Sc NMR for the analysis of molecular structure. Values of C_Q can be used to gauge the spherical symmetry of the ground-state electronic structure about a scandium nucleus, while the values of δ_{iso} and Ω can be used to provide information about the nature of the ligands that are bound to scandium and their

(73) Schurko, R. W.; Hung, I.; Macdonald, C. L. B.; Cowley, A. H. *J. Am. Chem. Soc.* **2002**, *124*, 13204.
(74) Hung, I.; Schurko, R. W. *Solid State Nucl. Magn. Reson.* **2003**, *24*, 78.
(75) Hung, I.; Schurko, R. W. *J. Phys. Chem. B* **2004**, *108*, 9060.
(76) Willans, M. J.; Schurko, R. W. *J. Phys. Chem. B* **2003**, *107*, 5144.
(77) Widdifield, C. M.; Schurko, R. W. *J. Phys. Chem. A* **2005**, *109*, 6865.

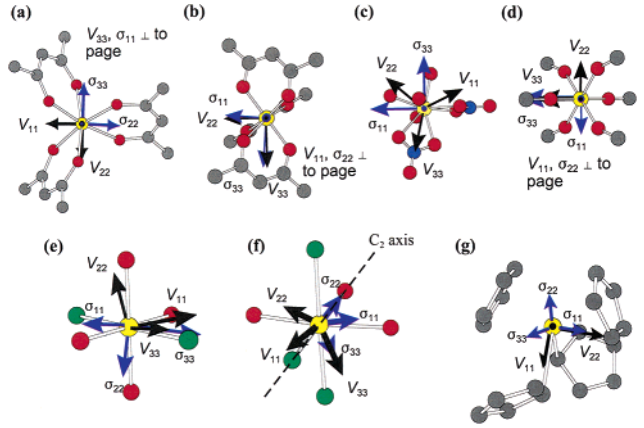

Figure 7. Proposed EFG and CS tensor orientations: (a) $Sc(acac)_3$; (b) $Sc(TMHD)_3$; (c) $Sc(NO_3)_3{\cdot}5H_2O$; (d) $Sc(OAc)_3$; (e) $ScCl_3{\cdot}6H_2O$; (f) $ScCl_3{\cdot}3THF$; (g) $ScCp_3$.

modes of bonding. The presence of symmetry elements, such as rotational axes and mirror planes, are reflected in the values of η_Q and κ, as well as in the Euler angles.

First Principles Calculations of ^{45}Sc Interaction Tensors. Ab initio calculations are performed to predict the orientations of the CS and EFG tensors in the molecular frames (Figure 7). This allows for relationships between the observed ^{45}Sc NMR parameters and molecular structure and symmetry to be confirmed and/or established. Calculated EFG and CS tensor parameters showing the best agreement with experimental values are presented for $Sc(acac)_3$, $Sc(TMHD)_3$, $Sc(NO_3)_3{\cdot}5H_2O$, $Sc(OAc)_3$, $ScCl_3{\cdot}6H_2O$, $ScCl_3{\cdot}3THF$, and $ScCp_3$ in Table 2. Calculations on $Sc(acac)_3$ employing the basis sets of Huzinaga[59] are shown in Table S3, and the results of all other calculations are shown in Table S4. Cartesian coordinate files containing the orientation of the EFG and CS tensors for each compound are provided in the Supporting Information.

$Sc(acac)_3$ and $Sc(TMHD)_3$. Calculations performed upon $Sc(acac)_3$ generally produce results which are in good agreement with the experimentally observed parameters. The B3LYP/6-311G** calculation on $Sc(acac)_3$ orients the largest component of the EFG tensor, V_{33}, and least shielded component of the CS tensor, σ_{11}, coincident with the pseudo-C_3 axis, in agreement with our proposed orientation on the basis of the experimental values of κ and η_Q. The theoretical Euler angles are found to be in excellent agreement with experimentally determined angles. Similar tensor orientations have been observed in $Co(acac)_3$ and $Al(acac)_3$, both of which have analogous molecular geometries.[78,79]

All calculations performed upon $Sc(TMHD)_3$ predict intermediate positive values of κ, distinct from the experimentally determined value of -0.7. V_{11} is the pseudo-unique component of the EFG tensor (Figure 7b) and is oriented near the pseudo-C_2 axis of the molecule and σ_{22}, while V_{33} and σ_{33} are nearly coincident and directed toward the bent ligands. The theoretical Euler angles are close to the observed angles (if β is near zero, α and γ are approximately interchangeable). The calculations are correctly predicting the orientation of the EFG and CS tensors within the molecular frame but consistently underestimate σ_{22} and overestimate σ_{33}.

(78) Reynhard, E. *J. Phys. C: Solid State Phys.* **1974**, *7*, 4135.
(79) Schurko, R. W.; Wasylishen, R. E.; Foerster, H. *J. Phys. Chem. A* **1998**, *102*, 9750.

$Sc(NO_3)_3{\cdot}5H_2O$ and $Sc(OAc)_3$. Calculations performed upon $Sc(NO_3)_3{\cdot}5H_2O$ yield several results which are close to the experimental values. There are no discernible symmetry elements present, with the exception of a pseudo-mirror plane, that could account for the observation of such a small value of C_Q. As mentioned earlier, the most reasonable explanations for the small C_Q, despite the lack of spherical symmetry, are the increased Sc−O distances. It is notable that V_{33} is oriented in the direction of one of the nitrogen atoms in a nitrate group (Figure 7c), though it is uncertain why this is the case. The calculated orientation of the CS tensor conforms to the symmetry of the atomic arrangement and is oriented such that the σ_{11} and σ_{33} are contained in the pseudo-mirror plane formed by the nitrate ligands.

In $Sc(OAc)_3$, calculations successfully predict that V_{33} and σ_{33} are the pseudo-distinct components (Figure 7d) and reveal that they are nearly collinear with the C_3 axis of the molecule. Thus, the tensors are aligned in the direction of chain propagation of this coordination polymer and are clearly constrained by the symmetry of the molecule. The predicted Euler angles are in excellent agreement with the experimental values.

$ScCl_3{\cdot}6H_2O$ and $ScCl_3{\cdot}3THF$. The experimental and theoretical parameters obtained for $ScCl_3{\cdot}6H_2O$ indicate that V_{11} and σ_{33} are the pseudo-unique components, and the value of α indicates they are not closely aligned (Figure 7e). The values of η_Q indicate that V_{11} is the pseudo-unique component and should be aligned along or near the C_4 axis of the molecule; however, this is not the case. The theoretical prediction aligns V_{33} at ca. 27° from the C_4 axis, with V_{11} and V_{22} oriented approximately 27 and 18° away from Sc−O bonds (C_2 axes), respectively. The theoretical CS tensor places σ_{33} along the Sc−Cl bond, approximately 26° from V_{33}, which is consistent with σ_{33} being the unique component of the CS tensor, while σ_{11} and σ_{22} are in the ScO_4 plane, oriented near the Sc−O bonds. Close agreement is observed between the experimental and predicted NMR tensor parameters and tensor orientations. It is worth noting that poor agreement is observed between the experimental values and those obtained from calculations upon a $[ScCl_2(H_2O)_4]^+$ unit if proton positions from the crystal structure are utilized (Table S5). Accordingly, EFG calculations employing optimized proton positions yield much better agreement with experimental values (Table S4).

The orientation of the CS tensor in $ScCl_3{\cdot}6H_2O$, which gives rise to high magnetic shielding along the Cl−Sc−Cl axis and deshielding in the ScO_4 plane, can be explained using Ramsey's description of contributions to paramagnetic shielding. The paramagnetic shielding tensor at a nucleus, A, is given as[80]

$$\sigma^{p}_{A\alpha\beta} = -\frac{\mu_0}{4\pi}\frac{e^2}{2m^2}\sum_{k\neq 0}(E_k - E_0)^{-1} \times$$

$$[\langle 0|\sum_i L_{i\alpha}|k\rangle\langle k|\sum_i \frac{L_{iA\beta}}{r_{iA}^3}|0\rangle + \langle 0|\sum_i \frac{L_{iA\alpha}}{r_{iA}^3}|k\rangle\langle k|\sum_i L_{i\beta}|0\rangle]$$

where $E_k - E_0$ is the energy difference between occupied ($\langle 0\rangle$) and virtual ($\langle k\rangle$) MOs and L_i and L_{iA} are the orbital angular momentum operators of the ith electron with respect to the gauge

(80) Ramsey, N. F. *Phys. Rev.* **1950**, *78*, 699.

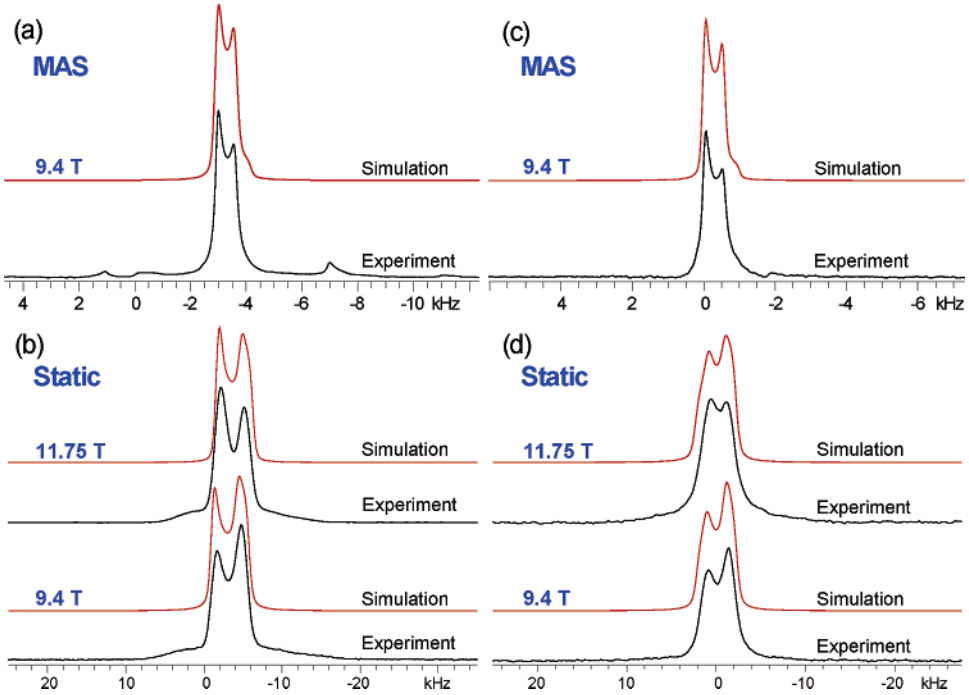

Figure 8. Solid-state ^{45}Sc NMR spectra and analytical simulations of $Sc(OTf)_3$ and ME-$Sc(OTf)_3$: (a) MAS spectrum of $Sc(OTf)_3$, $\nu_{rot} = 4$ kHz; (b) static spectra of $Sc(OTf)_3$ at 9.4 and 11.75 T; (c) MAS spectrum of ME-$Sc(OTf)_3$, $\nu_{rot} = 12$ kHz; (d) static spectra of ME-$Sc(OTf)_3$ at 9.4 T (AMDFS−Hahn echo) and 11.75 T.

origin and nucleus, respectively. The angular momentum operators describe the mixing of occupied and virtual MOs via rotation about an axis perpendicular to a plane containing the MOs, which can be visualized as physical rotation of charge about an applied magnetic field.

Magnetic shielding along the Cl−Sc−Cl axis is high since the occupied and virtual MOs in the ScO_4 plane are far apart in energy and do not have the appropriate symmetry for magnetic-dipole allowed mixing; as a result, the paramagnetic contribution to deshielding perpendicular to the ScO_4 plane is minimal. Conversely, deshielding arising from paramagnetic contributions in the plane are high, since there are energetically similar MOs of appropriate symmetry in the ScO_2Cl_2 planes which are available for mixing. The large Ω and high δ_{iso} are consistent with this qualitative model and are not observed in any of the complexes which do not have Sc−Cl bonds.

For $ScCl_3$·3THF, the calculated value of η_Q is in good agreement with the observed value and indicates that V_{33} is the pseudo-unique component of the tensor. V_{33} is nearly coincident with the Cl−Sc−Cl pseudo-axis ($\angle$174.5°), whereas V_{11} coincides with the C_2 axis of the molecule formed by O−Sc−Cl axis ($\angle$179.4°) (Figure 7f). It is important to note that σ_{33} is oriented near the Cl−Sc−Cl axis ($\perp$ to the $ClScO_3$ plane), σ_{22} near the Cl−Sc−O axis ($\perp$ to the Cl_2ScO_2 plane), and σ_{11} near the O−Sc−O axis ($\perp$ to the Cl_3ScO plane). This is consistent with arguments above, where the large paramagnetic deshielding contributions are generated perpendicular to the plane with the most coordinated Cl atoms. A detailed MO analysis is beyond the scope of the current study.

$ScCp_3$. Calculated and observed EFG parameters of $ScCp_3$ are in good agreement. Calculations were carried out using a $[ScCp_4]^-$ cluster (Figure 7g) and reveal that V_{11} is nearly coincident with one of the η^1-Cp−Sc bonds and that V_{33} is oriented in the direction of propagation of the metallocene polymer. The observation of a high value of η_Q, which indicates that V_{11} is the unique component of the EFG tensor, is not surprising in this context. It is difficult to comment on the observed CS tensor orientation; nonetheless, it is of interest to note that the calculations do predict a relatively large span. The predicted isotropic shifts fluctuate widely between the B3LYP and RHF calculations, perhaps suggesting that use of an isolated cluster in this instance is insufficient to properly model the CS tensor.

Summary of ab Initio Calculations. Inspection of all the calculations reveals that the RHF method is generally superior to the B3LYP method. The former typically result in both CS and EFG tensor parameters that are close to the experimentally observed values, while the latter do not correctly predict CS tensor parameters in most cases. In the case of extended systems (i.e., coordination polymers such as $Sc(OAc)_3$ and $ScCl_3$·$6H_2O$) calculations upon isolated small charged clusters are sufficient to accurately calculate the observed ^{45}Sc EFG and CS tensor parameters, indicating that the interactions are mainly intramolecular in origin. Examination of the calculated isotropic shifts reveals that the RHF calculations typically result in errors of less than ±25 ppm with larger basis sets (with the exception of $ScCp_3$), while the B3LYP calculations generally produce poorer agreement and greatly overestimate the effects of coordination by chlorine on chemical shifts.

Solid-State ^{45}Sc NMR Experiments on $Sc(OTf)_3$ and ME $Sc(OTf)_3$. Solid-State NMR of Microcrystalline (MC) $Sc(OTf)_3$. ^{45}Sc NMR spectra of MC-$Sc(OTf)_3$ and corresponding analytical simulations are shown in Figure 8. Simulations of MAS (Figure 8a) and static (Figure 8b) patterns yield C_Q = 4.7 MHz, $\eta_Q = 0.15$, $\delta_{iso} = -28$ ppm, $\Omega = 32$ ppm, and $\kappa = 0.3$. The static spectra possess rounded edges and do not terminate sharply into the baseline. This is most likely due to minor long-range disorder in the sample.

Table 3. Observed ^{45}Sc NMR Parameters of $Sc(OTf)_3$, ME $Sc(OTf)_3$, and $Sc(OAc)_3$

compound	C_Q (MHz)[a]	η_Q	δ_{iso} (ppm)	Ω (ppm)	κ	α (deg)	β (deg)	γ (deg)
$Sc(OTf)_3$	4.7(2)	0.15(5)	−28(1)	32(3)	0.3(1)	75(30)	18(4)	0(25)
ME-$Sc(OTf)_3$	4.2(2)	0.1(1)	1.8(3)	26(8)	−0.1(2)	90(30)	15(5)	0(25)
$Sc(OAc)_3$	4.6(2)	0.18(6)	−6.2(8)	73(5)	0.65(10)	0(45)	7(3)	90(45)

[a] See Table 1 for definitions of parameters.

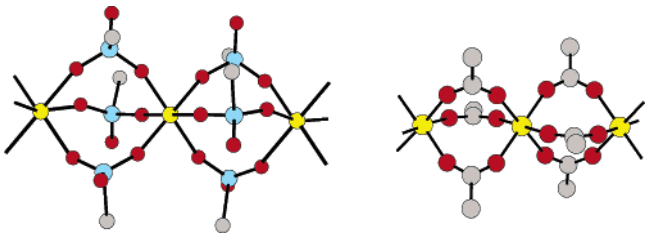

Figure 9. Model of $Sc(OTf)_3$ (left) and comparison to the structure of $Sc(OAc)_3$ (right). Fluorine and hydrogen atoms have been omitted for clarity.

There is currently no crystal structure of $Sc(OTf)_3$; however, the ^{45}Sc NMR data can be used to make structural inferences. The small C_Q suggests that the coordination environment of scandium must be of high symmetry, while the low Ω and negative isotropic chemical shift suggest that there is symmetric coordination by oxygen atoms from one type of ligand. The oxygen atoms should form a nearly idealized octahedron about the scandium center. Given the similarity of these parameters with those of $Sc(OAc)_3$ (Table 3), $Sc(OTf)_3$ should have a coordination polymer structure akin to that of $Sc(OAc)_3$. This is reasonable because triflate and acetate anions are similar in structure and can therefore coordinate to Sc in an equivalent manner. This is in accordance with the previously reported IR studies which suggests that the triflate ligands are bridging.[81] The structure of $Sc(OAc)_3$ is shown in Figure 9 along with a proposed model of $Sc_3(OTf)_3$. In addition, the solid-state ^{13}C and ^{19}F NMR spectra only contain one signal apiece (Figure S7), which is also consistent with the proposed structure (one type of carbon and fluorine atom). Thus, ^{45}Sc NMR spectroscopy can be applied as a rapid probe of structure and bonding in the context of the other systems examined within this work.

Solid-State NMR of Microencapsulated (ME) $Sc(OTf)_3$. The ^{45}Sc NMR spectra of ME-$Sc(OTf)_3$ reveal spectra similar to those observed from the microcrystalline sample (Figure 8c and 8d), with $\delta_{iso} = 1.8$ ppm, $C_Q = 4.2$ MHz, $\eta_Q = 0.1$, $\Omega = 26.0$ ppm, and $\kappa = -0.1$. A strong ^{1}H−^{45}Sc dipolar interaction (Figure S8) could not be completely decoupled in the static experiments at 11.75 T (Figure 8d), as evidenced by the lack of definition in the pattern. However, the visible discontinuities in the pattern are useful for the confirmation of the parameters obtained from the simulation of the spectrum acquired at 9.4 T. Comparison of the ^{45}Sc NMR parameters of $Sc(OTf)_3$ and ME-$Sc(OTf)_3$ (Table 3), the latter has a significantly higher chemical shift (scandium is less shielded) and a slightly smaller C_Q.

Kobayashi et al. have previously reported solution ^{45}Sc NMR data for $Sc(OTf)_3$ and ME-$Sc(OTf)_3$.[82] A positive chemical shift of ca. 30 ppm was observed in the solution ^{45}Sc NMR resonance of ME-$Sc(OTf)_3$ relative to that of $Sc(OTf)_3$, which was suggested to originate from an interaction between the benzene rings of the polystyrene and the scandium center. To further illustrate this, Kobayashi et al. acquired the solution ^{45}Sc NMR spectrum of $Sc(OTf)_3$ dissolved in 1,3,5-triphenylpentane and observed a positive chemical shift of 24 ppm with respect to the resonance of $Sc(OTf)_3$ dissolved in CD_3CN. Solid-state ^{45}Sc NMR experiments reveal that the chemical shift of the ME-$Sc(OTf)_3$ is +29.8 ppm with respect to that of the pure MC form, which is consistent with the solution NMR data of Kobayashi. The observation of similar ^{45}Sc EFG and CS tensor parameters, with the exception of the δ_{iso}, suggests that the structure of $Sc(OTf)_3$ remains fundamentally the same upon microencapsulation within polystyrene; most notably, the EFG parameters strongly suggest coordination of Sc by six bridging triflate ligands as well as retention of its coordination polymer structure. This is supported by the observation of similar IR spectra for both MC- and ME-$Sc(OTf)_3$.[17] The absence of a chemical shift close to that of MC-$Sc(OTf)_3$ also suggests that $Sc(OTf)_3$ is encapsulated at the molecular level; there is no large chemical shift distribution indicating the presence of nano- or microcrystalline domains.

The presence of ^{1}H−^{45}Sc dipolar coupling (likely from multiple proton sites) also indicates that there are protons close to the scandium atom (less than 4 Å). This observation is compatible with the proposal that there is an interaction between the benzene rings of the polystyrene and scandium; however, the nature of this interaction is not well defined. For most transition metals, interactions with aromatic π-systems typically result in magnetic shielding of the nucleus (i.e., a negative chemical shift), opposite to both solution and solid-state NMR observations. Interestingly, the ^{45}Sc nucleus might be unique in this respect, since large magnetic shielding effects are not observed in the π-coordinated $ScCp_3$ molecules.

The ^{19}F and ^{13}C NMR spectra of MC-$Sc(OTf)_3$ and ME-$Sc(OTf)_3$ support the ^{45}Sc NMR data, suggesting that the ligands are not significantly changed and the fundamental coordination polymer structure is retained upon microencapsulation. The ^{19}F NMR spectra of MC-$Sc(OTf)_3$ and ME-$Sc(OTf)_3$ (Figure S7a) have identical chemical shifts at ca. −77(1) ppm. As well, in the ^{13}C Hahn-echo and ^{19}F−^{13}C VACP/MAS NMR spectra of each system, the CF_3 resonances are the same at 118 ppm (Figure S7b,c). The CF_3 carbon resonance is not visible in the ^{1}H−^{13}C VACP/MAS spectra of ME-$Sc(OTf)_3$, which indicates that CP is inefficient at this high spinning speed; however, at lower spinning speeds where ^{1}H−^{13}C VACP would be more efficient, the CF_3 resonance is broadened beyond ready detection by large ^{19}F−^{13}C dipolar couplings. Correspondingly, the polystyrene peaks are only observed in the ^{13}C Hahn-echo and ^{1}H−^{13}C VACP/MAS NMR spectra, for similar reasons.

Conclusions

The ^{45}Sc NMR interaction tensor parameters have been measured for a number of well-characterized scandium compounds possessing a broad range of metal coordination environments. For the first time, clear relationships are drawn between

(81) Hamidi, M. M.; Pascal, J. *Polyhedron* **1993**, *13*, 1787.
(82) Kobayashi, K. *Chem. Commun.* **2003**, *2003*, 449.

the scandium coordination environments and the nature of the ^{45}Sc NMR interaction tensors. EFG tensor parameters are primarily affected by the geometry of the scandium coordination environment, while CS tensor parameters are affected by both the symmetry of the coordination environment and nature of bonding in the first coordination sphere. Anisotropic chemical shielding of the scandium nucleus is observed in all of the systems and plays a significant role in defining the scandium chemical shift range. Ab initio calculations of the CS and EFG tensor parameters are in very good agreement with experimental data. In addition, the predicted tensor orientations within the molecular frames aid in rationalizing the origin of the observed CS and EFG tensor parameters. Solid-state ^{45}Sc NMR spectroscopy has also been successfully applied to structurally characterize two systems for which single-crystal X-ray diffraction data is unavailable and/or unobtainable. It has been demonstrated that $Sc(OTf)_3$ is a coordination polymer that possesses a structure similar to $Sc(OAc)_3$ and that this structure is fundamentally the same upon microencapsulation in polystyrene. However, the distinct chemical shift and significant ^{1}H−^{45}Sc dipolar couplings observed in the ^{45}Sc NMR spectra of ME-$Sc(OTf)_3$ is consistent with the proposal that immobilization is due to an interaction between the scandium center and the phenyl groups of the polystyrene.

Acknowledgment. This research was funded by the Natural Sciences and Engineering Research Council (NSERC, Canada) and Imperial Oil. A.J.R. thanks NSERC for an Undergraduate Summer Research Award and the Ontario Ministry of Training, Colleges, and Universities for an Ontario Graduate Scholarship. R.W.S. is also grateful to the Canadian Foundation for Innovation (CFI), the Ontario Innovation Trust (OIT), and the University of Windsor for funding the Solid-State NMR Facility at the University of Windsor. We thank Dr. Warren Piers and Korey Conroy (University of Calgary) for synthesis of $Sc(acac)_3$ and $ScCl_3$·3THF. Mr. Mike Fuerth is thanked for his assistance with experiments at 11.75 T. Dr. Charles L. B. Macdonald is thanked for his assistance with single-crystal X-ray diffraction experiments and the refinement of crystal structures.

Supporting Information Available: Cartesian coordinate files of EFG and CS tensor orientations within molecular frames, CIF files of the single-crystal X-ray diffraction structures of $Sc(TMHD)_3$, $Sc(NO_3)_3$·$5H_2O$, and $ScCl_3$·$6H_2O$, tables of the experimental NMR parameters employed, tables of X-ray crystallographic data, tables of ab initio calculation results, ^{45}Sc NMR spectra without ^{1}H decoupling, powder X-ray diffraction patterns, ^{13}C and ^{19}F NMR spectra, and the complete ref 57. This material is available free of charge via the Internet at http://pubs.acs.org.

JA060477W